A Phenomenological Model for Predicting Fatigue Life in Bovine Trabecular Bone

P. Ganguly[†]
T. L. A. Moore[‡]
L. J. Gibson[†*]

[†]Department of Materials Science and Engineering,
Massachusetts Institute of Technology,
Cambridge, MA 02139
[‡]Exponent Failure Analysis Associates, Inc.
Philadelphia, PA 19104

Cyclic loading of bone during daily activities can lead to fatigue degradation and increased risk of fracture in both the young and elderly population. Damage processes under cyclic loading in trabecular bone result in the reduction of the elastic modulus and accumulation of residual strain. These effects increase with increasing stress levels, leading to a progressive reduction in fatigue life. The present work analyzes the effect of stress and strain variation on the above damage processes in bovine trabecular bone, and develops a phenomenological model relating fatigue life to the imposed stress level. The elastic modulus reduction of the bone specimens was observed to depend on the maximum compressive strain, while the rate of residual strain accumulation was a function of the stress level. A model was developed for the upper and lower bounds of bone elastic modulus reduction with increasing number of cycles, at each stress range. The experimental observations were described well by the model. The model predicted the bounds of the fatigue life with change in fatigue stress. The decrease in the fatigue life with increasing stress was related to corresponding increases in the residual strain accumulation rates at the elevated stress levels. The model shows the validity of fatigue predictions from relatively few cyclic experiments, by combining trends observed in the monotonic and the cyclic tests. The model also presents a relatively simple procedure for predicting the endurance limit for bovine trabecular bone specimens. [DOI: 10.1115/1.1762893]

1 Introduction

Repetitive, cyclic loading of bone during the daily course of activities is one of the primary causes of bone fracture in humans [1–2]. Such fatigue fractures can occur both in healthy adults (stress fractures) [3] and in the elderly population (fragility fractures) [4]. Stress fractures can be caused by prolonged and intense regular exercise, e.g. in military recruits, athletes or ballet dancers [5–6]. On the other hand, fragility fractures in the elderly generally result from a reduction in bone strength due to osteoporosis [7]. Both stress and fragility fractures have been associated with trabecular bone. Stress fractures have been observed in trabecular bone at the neck of the femur and the proximal tibia [3]. Fragility fractures have been observed in the proximal femur, and are particularly prevalent in the vertebrae, where the trabecular bone carries most of the load [8].

Compressive fatigue failure in trabecular bone has been experimentally investigated by a number of researchers [9–13]. In these experiments, trabecular bone specimens were loaded under cyclic compression to predefined normalized stress levels (stress normalized by intact elastic modulus of the specimen). The fatigue life (number of cycles corresponding to a 5% or 10% loss in elastic modulus) of trabecular bone was observed to decrease with an increase in the fatigue stress level [9–11]. The mechanical response of the trabecular bone under fatigue was characterized by a decrease in the elastic modulus [9–11] and an increase in the residual strain with increasing number of cycles (and increasing maximum strain) [10–11]. The decrease in the elastic modulus has generally been related to increasing damage in trabecular bone, in the form of microcracking and fracture in the trabeculae, under both cyclic [13] and monotonic compression loadings [14]. Changes in modulus in cortical bone have also been associated with microcrack accumulation [15–17]. The experimentally observed increase in the residual strain with increasing number of cycles was originally attributed to creep processes [10]. However, recent investigations have revealed that creep may be responsible for only a small fraction of the total residual strain observed in fatigue experiments [18]. These two phenomena, namely the reduction of elastic moduli and increase in residual strain, may determine the fatigue life of trabecular bone. Thus, development of models relating these phenomena to loading variables (e.g. stress, strain) is necessary for a predictive understanding of fatigue life variations in the trabecular bone under different loading conditions.

Fatigue processes in trabecular bone have been modeled using finite element methods applied to regular [19] and random 2-D [20] and 3-D cellular solids [21]. The growth of pre-existing cracks under fatigue was assumed to follow the Paris law [22]. The models showed that failure of a small fraction of the trabeculae could lead to significant reduction in the bone modulus, and predicted a decrease in the fatigue life with increasing normalized stress range. However, the rate of change of fatigue life (with change in stress) predicted by the models was lower than that observed in experiments. In addition, the models did not account for the residual strain accumulation in the bone specimens. Carter and Caler [23–24] have modeled the secant modulus loss for cortical bone in terms of cycle-dependent (fatigue) and time-dependent (creep) components, with the former dominating at high normalized stresses, and the latter at relatively low normalized stresses. However, as mentioned above, creep processes may not be significant in compressive fatigue of trabecular bone, and Moore and Gibson [11] have shown that trabecular bone specimens tested to similar number of cycles (in compressive fatigue) did not exhibit a similar loss in modulus, but produced similar residual strains. Taylor [25] has modeled fatigue crack growth in cortical bone by differentiating the cracks into long and short cracks, and defining separate growth laws for each crack group, thereby accounting for microstructural barriers that the crack may need to overcome while growing. Taylor's model has been relatively successful in predicting the fatigue life for cortical bone. However, in case of trabecular bone, such a model may only be invoked to model crack growth in individual trabeculae, and its

*Corresponding author.

Contributed by the Bioengineering Division for publication in the JOURNAL OF BIOMECHANICAL ENGINEERING. Manuscript received by the Bioengineering Division August 1, 2003; revision received October 27, 2003. Associate Editor: L. Setton.

use to predict the trabecular bone fatigue life may be cumbersome. Thus, a different approach is necessary to model the fatigue life in trabecular bone.

The objective of the present study is to develop a predictive model for fatigue life as a function of the independent experimental variables (stress, strain). The changes in the specimen modulus and the residual strain were determined for cyclic compressive loading at different normalized stresses. Since failure in trabecular bone has generally been defined as a 5–10% loss in secant modulus [19–21], the analysis was restricted to a maximum compressive strain of 0.015, where all the specimens were observed to exhibit a 10% (or more) loss in secant modulus. In order to investigate the effect of loading conditions, the specimen modulus variation observed in monotonic compression was compared to that in cyclic experiments. The phenomenological equations relating the modulus and the residual strain in the trabecular bone specimens to the experimental variables (stress and strain) were developed from the experimental analysis. The equations were later incorporated into a fatigue life model, and the number of cycles that the bone specimens could withstand prior to failure at different normalized stresses was predicted. The analysis further explores the possibility of fatigue characteristic predictions based on relatively few cyclic experiments, and develops an analytical formulation for estimating the endurance limit of bovine trabecular bone.

2 Experimental Methodology

2.1 Monotonic Compression Tests. Tests were performed on waisted cylindrical specimens obtained from bovine proximal tibia, following the method of Keaveny et al. [26]. The methodology for the monotonic compression tests has been detailed by Moore and Gibson [14]. The specimens had a nominal diameter of 6 mm and a nominal gage length of 5 mm. The specimens were selected so that the axis of the trabecular bone was aligned with the longitudinal axis of the specimen. Each specimen was compressed under strain control (at a strain rate of 0.5 s^{-1}), to maximum compressive strains ranging from 0.004 to 0.04.[1] A miniature extensometer (Model 632-29C-30, MTS, Eden prairie, MN) was mounted centrally at the gage length. The initial modulus, E_0^m, for each specimen was determined by fitting a linear curve to the initial portion ($\varepsilon = 0.001$ to 0.004) of the compressive stress-strain curve (Fig. 1) [27]. The secant moduli (E_{sec}^m) of the specimens at higher strains (i.e., $\varepsilon > 0.004$) were also calculated, and were normalized by the initial modulus. For each of the specimens, the E_{sec}^m/E_0^m was plotted against strain. The best-fit line was estimated over the strain range where $E_{\text{sec}}^m/E_0 < 1$, and generally involved 30–100 data points. The analysis was restricted to a maximum strain of 0.015, which corresponded to a secant modulus loss of greater than 10%.

2.2 Cyclic Compression Tests. The methodology for the cyclic compression tests has been detailed in Moore and Gibson [11]. The tests were performed on cylindrical specimens of bovine trabecular bone taken from the proximal tibia, following the method of Keaveny et al. [28]. The specimen gage length was approx. 9 mm, and the diameter was 6.27 mm. A small compressive pre-load (~50 N) was placed on the specimen to ensure contact between the loading platens. A 0.5-inch (12.7 mm) extensometer (Instron 2620-826, Instron Corp., Canton, MA) was attached to the specimen ends. Following Keaveny et al. [28], this method of modulus measurement was expected to yield similar results as in the monotonic compression tests, which used waisted specimens with a miniature extensometer attached directly to the specimen gage length. Prior to fatigue testing, the specimen was preconditioned by loading for 10 cycles in strain control using a sinusoidal waveform from 0.0 strain to 0.003 strain at a frequency

[1]A positive sign convention for compressive stresses and strains has been used in this work.

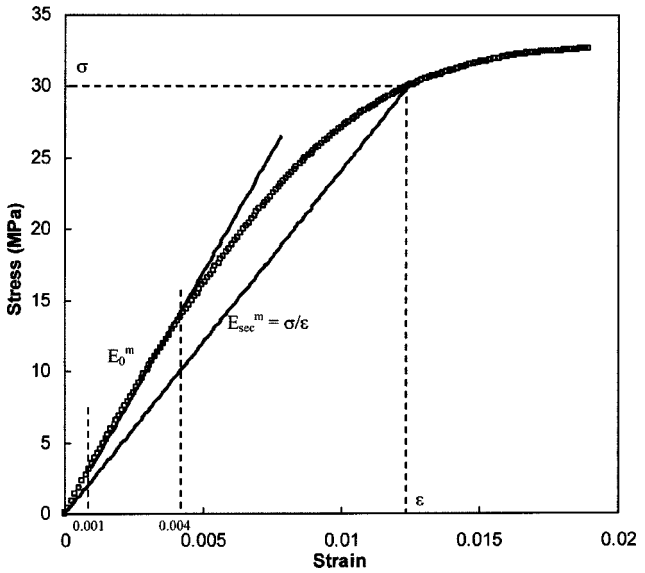

Fig. 1 A characteristic stress-strain curve for bovine trabecular bone under monotonic compression. The initial modulus (E_0^m) was calculated by the best-fit line in the strain range 0.001–0.004. The secant modulus (E_{sec}^m) at higher strains were calculated by the ratio of the stress and strain.

of 2.0 Hz. The initial modulus (E_0^f) was measured by taking the slope of the best linear fit of the tenth loading cycle from 0.001 to 0.003 strain. The fatigue tests were performed under load control at a frequency of 2.0 Hz. Specimens were loaded from the nominal compressive preload (~50 N) to a predetermined load corresponding to a normalized stress level, $\Delta\sigma/E_0^f$. Normalized stress was used instead of stress to reduce the scatter in the results caused by large variations in the initial modulus associated with density variations in the trabecular bone.

The cyclic tests were performed at four nominal normalized stress levels ($\Delta\sigma/E_0^f = 0.005$, 0.006, 0.007 and 0.008). However, the loads in the actual experiments were generally slightly higher than the prescribed load. The overload was dependent on the sensitivity of the load controller, and in the present set of experiments, was ~30–50 N. This translated to the experimentally detected normalized stress levels generally being ~0.0003–0.0011 higher than prescribed. Depending on the experimentally determined normalized stress, the cyclic stress-strain diagrams were grouped into four groups: (a) $0.005 < \Delta\sigma/E_0^f \leq 0.006$, (b) $0.006 < \Delta\sigma/E_0^f \leq 0.007$, (c) $0.007 < \Delta\sigma/E_0^f \leq 0.008$ and (d) $0.008 < \Delta\sigma/E_0^f \leq 0.009$. The cyclic stress-strain diagrams were analyzed to determine:

a. decrease in the secant modulus of the specimen with increasing strain,
b. accumulation of residual strain per cycle.

The secant modulus (Fig. 2) for each cycle was calculated from the loading part of the curve and was defined by

$$E_{\text{sec}}^f = \frac{\sigma_{\max} - \sigma_{\min}}{\varepsilon_{\max} - \varepsilon_{res}} \tag{1}$$

where $\sigma_{\max}$ and $\varepsilon_{\max}$ were the maximum stress and strain recorded during the cycle, and $\sigma_{\min}$ and ε_{res} were the minimum stress and the residual strain at the beginning of the cycle. The secant modulus was normalized by the initial modulus (E_0^f), to determine the normalized secant modulus (E_{sec}^f/E_0^f). Preliminary analysis suggested that the rate of residual strain accumulation with the number of cycles was relatively high for the first few cycles (1–5 cycles), but was subsequently relatively constant. The cyclic com-

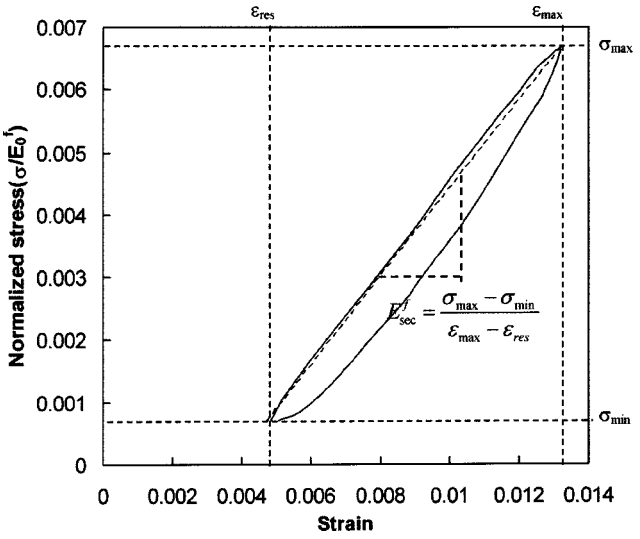

Fig. 2 Calculation of the secant modulus for a given cycle for a sample tested at a maximum compressive normalized stress (σ/E_0^f) of 0.0066.

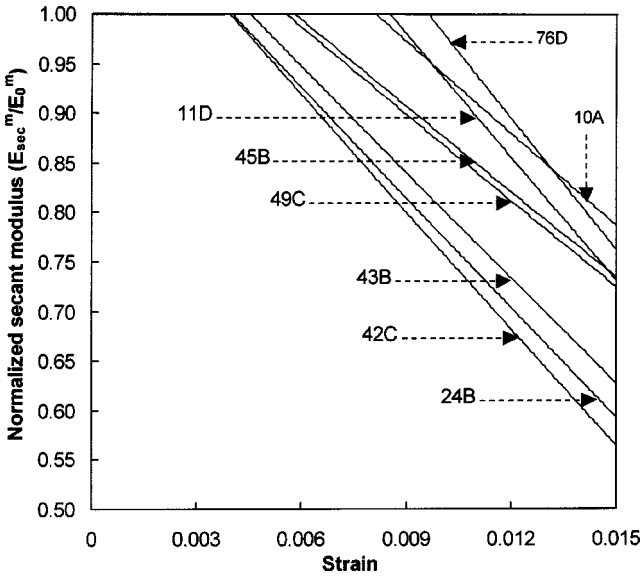

Fig. 3 Variation of the normalized secant modulus with increasing strain for representative specimens under monotonic compression. The secant modulus variation for each sample has been represented by the best-fit linear plot.

pression data were analyzed for every cycle for the first five cycles for all specimens. For subsequent cycles, the frequency of data analysis depended on the normalized stress level, and the number of cycles for each test. Typically, the data were analyzed every 2–20 cycles for tests at normalized stresses higher than 0.006, while for tests at lower normalized stresses, it was analyzed every 20–200 cycles. For each cycle analyzed, the secant modulus and the residual strain were plotted against the maximum strain for that cycle (ε_{max} in Fig. 2).

The cyclic compression tests were conducted such that the tests continued till the specimens reached a prescribed maximum strain level, varying from 0.008 to 0.025 [11]. The reduction of the normalized secant modulus observed at the lowest prescribed strain level (0.008) was often less than that required for the present purposes (10% reduction or more). The analysis of the data from experiments undertaken at this maximum strain level has not been included in the present work. The analysis of the remaining data (for 89 specimens) was restricted to a maximum strain of 0.015, the modulus reduction observed at this strain level being more than 10%. Fifteen specimens exhibited a normalized secant modulus greater than 1 for several cycles (10 or more cycles or until the end of the test) during the cyclic loading. The E_0^f for these specimens were assumed underestimated, and these specimens were excluded from the analysis. In addition, for four specimens, the minimum stress at the end of the cycles was significantly higher than the prescribed preload (~60–70 N instead of ~50 N). This discrepancy gave rise to high residual strains, and presented problems in residual strain analysis. The analysis for these specimens was excluded from the present work.

3 Data Analysis

3.1 Reduction in Secant Modulus Under Monotonic and Cyclic Compression. Figure 3 shows the best-fit lines for the variations in the normalized secant modulus (E^m_{sec}/E^m_0) with increasing strain, under monotonic compressive loading.[2] At low strains, the secant moduli for all the specimens were similar to the initial (undamaged) modulus. The best-fit lines were fit over the strain range where $E_{sec}/E_0 < 1$, and yielded R^2 values greater than 0.98. Moore and Gibson [14] have shown that the reduction in the secant moduli can be correlated with damage accumulation in the trabecular bone specimens. The compression specimens appear to be relatively damage-free at low levels of compressive strains. The damage initiation strain (i.e., the strain beyond which the specimen secant modulus was consistently lower than the initial modulus, estimated from the intercept of the best-fit lines on the line $E^m_{sec}/E^m_0 = 1$) differed from specimen to specimen, ranging from a minimum of 0.0038 to maximum of 0.0097. This variation is similar to that observed by Moore and Gibson [14], who used a different technique to estimate the point of nonlinearity in the present set of monotonic stress-strain curves (intersection of the specimen stress-strain curve with a line whose slope was equal to 95% of the specimen initial modulus). The overall variation of the normalized secant modulus (E^m_{sec}/E^m_0) with increasing strain was influenced by (a) the damage initiation strain, and (b) the rate of normalized secant modulus decrease with increasing strain. The rate of normalized secant modulus decrease for the different specimens were determined from the slopes of the E^m_{sec}/E^m_0 vs. strain plots shown in Fig. 3, and the maximum slope was approximately 1.5 times the minimum slope. For most of the specimens, the damage initiation strain dominated the overall secant modulus variation. For example, seven (76D, 11D, 45B, 49C, 43B, 24B and 42C) of the eight specimens shown in Fig. 3 approximately preserved their relative positions, with the lower damage initiation strain yielding a lower response.

Figure 4(*a*)–(*d*) shows the variation of the normalized secant modulus (E^f_{sec}/E^f_0) with increasing strain, for specimens tested under cyclic compression at $\Delta\sigma/E^f_0$ ranges of (0.005, 0.006],[3] (0.006, 0.007], (0.007, 0.008] and (0.008, 0.009], respectively. The upper and lower bounds of the curves from the monotonic compression tests have also been included for comparison. Some of the cyclic compression data points fell outside the bounds defined by monotonic compression. However, given the intrinsic wide variability (specimen-to-specimen) in the trabecular bone normalized secant modulus at a given strain, the difference be-

[2]Note that Fig. 3 shows representative curves from the specimens tested under monotonic compression. The specimens showed in Fig. 3 were loaded to strains higher than 0.015. The analysis for specimens that were loaded to strains lower than 0.015 were similarly undertaken, though restricted to the respective maximum strains.

[3]This signifies a range which is open at the lower bound and closed at the upper bound, i.e. when normalized stress is greater than 0.005, but less than or equal to 0.006.

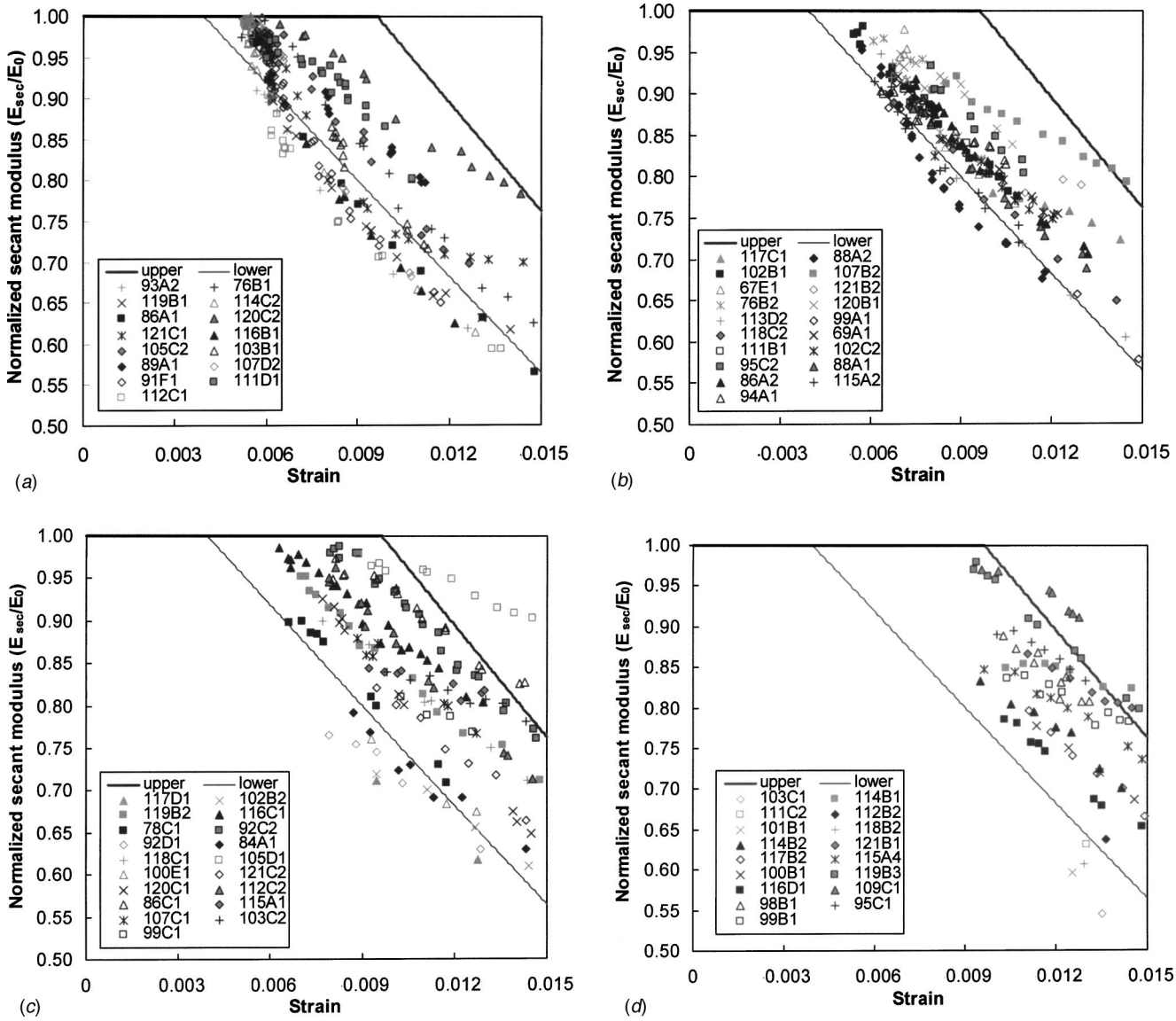

Fig. 4 Variation of secant moduli with increasing strain for the trabecular bone samples at normalized stress ($\Delta\sigma/E_0^f$) ranges of (*a*) (0.005, 0.006], (*b*) (0.006, 0.007] (*c*) (0.007, 0.008] and (*d*) (0.008, 0.009]. The experimental points have been identified by the sample numbers. The upper and lower bounds from the monotonic tests have been included for comparison, and shown in the plots by the solid lines (upper and lower).

tween the monotonic compression and the cyclic compression bounds seen minimal. The reduction in the normalized secant modulus for bovine trabecular bone appears to be similar under cyclic and monotonic compression loadings.[4] Thus, the reduction in specimen modulus with increasing strain seems to be governed by the intrinsic characteristics (e.g. trabecular architecture and material properties) of the trabecular bone specimens, rather than the loading (or extrinsic) characteristics.

The similarity in the secant modulus vs. strain curves under monotonic and cyclic loadings also suggests a macroscopic strain-based failure criterion for the trabecular bone specimens. The monotonic compression tests were conducted under strain control, while the cyclic tests were conducted under stress control. The bone specimens were exposed to much lower normalized stresses under cyclic loading, as compared to that under monotonic loading. The similarity in the secant modulus degradation under monotonic and cyclic loadings thus precludes a primarily stress-based criterion. In addition, the similarity in effect of cyclic and monotonic (non-cyclic) loading indicates that the failure criterion is not based on the number of cycles.

3.2 Accumulation of Residual Strain. Figure 5 shows typical plots of accumulated residual strain with increasing number of cycles, for typical cyclic compression specimens tested in the normalized stress ranges of (0.005, 0.006], (0.006, 0.007], (0.007, 0.008] and (0.008, 0.009]. For all the specimens, the plots contained two phases:

a. primary phase, characterizing the initial part of the residual strain accumulation curve. Typically, this phase consisted of 2–5 cycles for specimens tested in the normalized stress range (0.005, 0.006], and 1–2 cycles for specimens tested at higher normalized stress levels. The average residual strain accumulation rate (i.e., change in residual strain per cycle) during this phase was high, relative to that observed later in the test. The magnitude of the residual strain accumulated in the primary phase were similar for

[4]The superscripts *f* and *m* differentiating the elastic modulus under fatigue and monotonic loadings are henceforth removed, and the symbols E_0 and E_{sec} will indicate initial and secant elastic modulus under either loading condition.

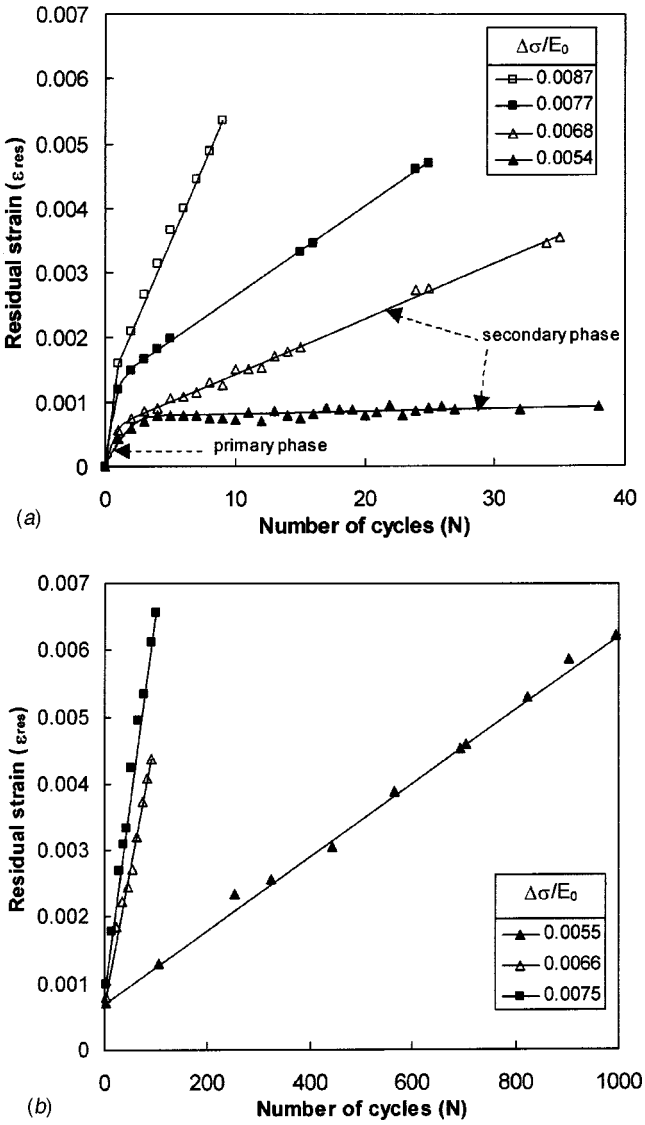

Fig. 5 Plots showing the accumulation of total residual strain with increasing number of cycles, for typical samples in the (0.005, 0.006], (0.006, 0.007], (0.007, 0.008] and (0.008, 0.009] normalized stress ranges. (*a*) The initial part of the residual strain plots, showing the primary and the secondary phases. (*b*) The secondary residual strain evolution at large number of cycles. The plot for $\Delta\sigma/E_0=(0.008,0.009]$ has been omitted from (*b*), the fatigue life at that stress level being comparable to the number of cycles shown in (*a*). Note that the residual strain analysis for the same normalized stress range shown in (*a*) and (*b*) corresponds to different specimens.

tests conducted in the (0.005, 0.006] and (0.006, 0.007] normalized stress ranges, while those for tests conducted in the (0.007, 0.008] and (0.008, 0.009] ranges were slightly higher (see Fig. 5(*a*)).

b. secondary phase, consisting of the residual strain accumulation in the subsequent cycles. For each fatigue specimen, the rate of secondary residual strain accumulation was relatively constant in the strain range analyzed in the present work ($\varepsilon \leqslant 0.015$). The characteristic value of the secondary residual strain accumulation per cycle for each specimen was obtained from the best-fit line through the plot of residual strain vs. number of cycles in the secondary phase (see Fig. 5(*a*) and (*b*)).

Table 1 shows the maximum, minimum and median rates of secondary residual strain accumulation rates for tests conducted in the normalized stress ranges of (0.005, 0.006], (0.006, 0.007], (0.007, 0.008] and (0.008, 0.009]. Considerable difference between the maximum and the minimum rates at the same normalized stress range is evident. Figure 6 shows the secondary residual strain accumulation rates for all the specimens, as a function of the measured normalized stress. A power-law curve fits the data well. The curves indicate that the secondary residual strain accumulation rate is a function of normalized stress, generally increasing with an increase in the normalized stress. The approximate upper and lower bounds of the secondary residual strain variation with normalized stress are also shown (Fig. 6).

For any given trabecular bone specimen under cyclic loading, an important characteristic is the fatigue life, or the number of cycles to failure, defined here as the number of cycles to reach a predetermined loss of modulus. The experimental analysis presented above shows that:

- the normalized secant modulus is governed by maximum strain,
- the secondary residual strain accumulation rate is governed by the normalized stress.

Thus,

$$\frac{E_{\text{sec}}}{E_0} = f_1(\varepsilon_{\max}) \tag{2}$$

$$\frac{d\varepsilon_{res}^{\text{sec}}}{dN} = f_2(\Delta\sigma/E_0) \tag{3}$$

where $d\varepsilon_{res}^{\text{sec}}/dN$ is the residual strain accumulation per cycle in the secondary phase, N is the number of cycles and f_1 and f_2 are experimentally determined functions.

For any given cycle,

$$\varepsilon_{\max} = \varepsilon_{res} + \frac{\Delta\sigma}{E_{\text{sec}}} \tag{4}$$

Table 1 Summary of the cyclic loading tests, showing the maximum, minimum and median values for the residual strain accumulation characteristics in the primary and the secondary phase. Note that the different quantities in any given row do not necessarily correspond to the same specimen.

Nominal bounds on maximum normalized stress (Min/Max)	Experimentally measured maximum normalized stress bounds (Min/Max)	Residual strain at end of primary phase (Min/Max (Median))	Rate of secondary residual strain accumulation (/cycle) (Min/Max (Median))
0.005/0.006	0.0053/0.0059	0.0006/0.0012 (0.0007)	$2\times10^{-6}/4\times10^{-5}$ (5×10^{-6})
0.006/0.007	0.0061/0.0069	0.0004/0.0025 (0.0007)	$5\times10^{-6}/2\times10^{-4}$ (4×10^{-5})
0.007/0.008	0.0072/0.008	0.0006/0.0035 (0.0011)	$1\times10^{-5}/1\times10^{-3}$ (1×10^{-4})
0.008/0.009	0.0083/0.0087	0.0010/0.0035 (0.0013)	$1\times10^{-4}/2\times10^{-3}$ (4×10^{-4})

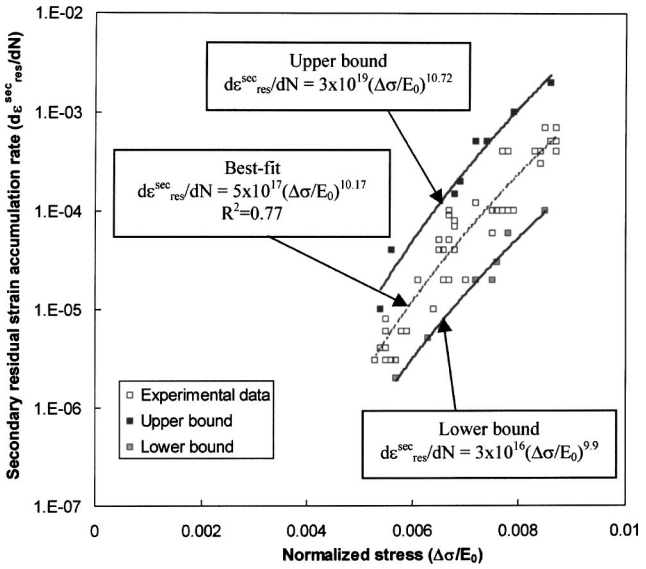

Fig. 6 Experimentally observed variation in the secondary residual strain accumulation rate with changes in normalized stress. The best-fit line was obtained by fitting a power-law curve on the entire experimental data (open, solid and gray squares). The points that appear to be bounding the data were identified (upper bound: solid squares, lower bound: gray squares) and separate power-law curves were fit to obtain the upper and lower bound variation equations.

The residual strain can be divided into the primary and secondary (constant) components. If ε_{res}^{pr} is the primary residual strain and $d\varepsilon_{res}^{\sec}/dN$[5] is the secondary residual strain accumulation rate (per cycle) then,

$$\varepsilon_{\max}=\left(\varepsilon_{res}^{pr}+N^{\sec}\frac{d\varepsilon_{res}^{\sec}}{dN}\right)+\frac{\Delta\sigma}{E_{\sec}} \tag{5}$$

where $N^{\sec}$ is the number of cycles in the secondary phase.

Substituting Eqs. (2) and (3) into Eq. (5),

$$f_1^{-1}(E_{\sec}/E_0)=\varepsilon_{res}^{pr}+N^{\sec}f_2(\Delta\sigma/E_0)+\frac{\Delta\sigma}{E_{\sec}} \tag{6}$$

$$N^{\sec}=N-N^{pr} \tag{7}$$

where N and N^{pr} are the total number of cycles and the number of cycles in the primary residual strain accumulation phase respectively. Putting Eq. (7) in Eq. (6) and rearranging,

$$f_1^{-1}(E_{\sec}/E_0)-\frac{(\Delta\sigma/E_0)}{(E_{\sec}/E_0)}=\varepsilon_{res}^{pr}+(N-N^{pr})f_2(\Delta\sigma/E_0) \tag{8}$$

Given that N^{pr} represents a relatively small number of cycles (1–5 in the normalized stress range analyzed here) and is approximately known, Eq. (8) would yield the functional form of variation of the normalized secant modulus ($E_{\sec}/E_0$) with N, for cyclic tests at constant normalized stresses ($\Delta\sigma/E_0$). The relationship between $E_{\sec}/E_0$ and N as shown in Eq. (8) is nonlinear. The exact nature of the relationship would depend on the functions f_1 and f_2. For a given trabecular bone specimen, f_1 can be evaluated from the $E_{\sec}/E_0$ vs. strain plot for that specimen (shown in Fig. 4), while the corresponding f_2 is shown in Fig. 6. Both f_1 and f_2 are material dependent and vary from specimen to specimen, and the $E_{\sec}/E_0$ vs. N curves are expected to be different for different specimens. However, the upper and lower bounds for the curves may be constructed by evaluating Eq. (8) for suitable bounding f_1 and f_2 functions. The bounds for $E_{\sec}/E_0$ vs. N variation may be used as a characteristic for bovine trabecular bone. A numerical model for determining such bounds for $E_{\sec}/E_0$ vs. N curves is developed in the next section.

4 Numerical Model: Development and Results

4.1 Choice of Suitable Bounds for f_1 and f_2. The function f_1, which relates the change in normalized secant modulus ($E_{\sec}/E_0$) with strain, was observed to be similar for monotonic and cyclic compression tests. The normalized secant modulus variation determined from cyclic compression experiments generally fell inside or around the monotonic compression bounds (see Fig. 4). The upper and lower bounds for the f_1 function were thus approximated by the respective bounds from the monotonic experiments. The bounding functions were:

- Upper bound (defined by curve 76D in Fig. 3)

$$\text{For } \varepsilon\leqslant 0.0097: \quad E_{\sec}/E_0=1.0$$
$$\text{For } \varepsilon>0.0097: \quad E_{\sec}/E_0=1.43-44.38\varepsilon \tag{9}$$

- Lower bound (defined by curve 42C in Fig. 3)

$$\text{For } \varepsilon\leqslant 0.0038: \quad E_{\sec}/E_0=1.0$$
$$\text{For } \varepsilon>0.0038: \quad E_{\sec}/E_0=1.15-39.41\varepsilon \tag{10}$$

The value of the function f_2, which defines the rate of accumulation of secondary residual strain, depended on the normalized stress level at which the cyclic compression experiments were conducted. The upper and lower bounds of f_2 for different normalized stresses have been shown in Fig. 6, while experimentally determined bounding values of f_2 for a given normalized stress range are shown in Table 1.

To determine which combination of the bounding functions f_1 and f_2 would yield the upper bound (and the lower bound) for $E_{\sec}/E_0$ vs. N curves, Eq. (8) may be rewritten as:

$$N=\frac{\varepsilon_{\max}-\varepsilon_{res}^{pr}-\dfrac{(\Delta\sigma/E_0)}{f_1(\varepsilon_{\max})}}{f_2(\Delta\sigma/E_0)}+N^{pr} \tag{11}$$

Eq. (11) shows that a combination of high f_1 and low f_2 would yield the maximum value of N, for a given $\varepsilon_{\max}$, ε_{res}^{pr}, $\Delta\sigma/E_0$ and N^{pr}. Thus, the upper bound of f_1 and the lower bound of f_2 were used for the modeling the upper bound $E_{\sec}/E_0$ vs. N curve. On the other hand, the lower bound of f_1 and the upper bound of f_2 were used in the lower bound $E_{\sec}/E_0$ vs. N model.

4.2 Model Development. The cyclic stress-strain curves were generated based on Eq. (5). In each normalized stress range, curves representing the upper and lower bound behavior of the bovine trabecular bone specimens were generated. For each cycle, both the loading and the unloading curves were defined. For each loading curve, an initial zero-stress state was assumed. The loading curve was constructed by prescribing normalized stress increments ($d\sigma/E_0$) equal to 1/10th of the maximum normalized stress ($\Delta\sigma/E_0$), and calculating the corresponding strain increments ($d\varepsilon$) from the incremental formulation of Eq. (5). The strain at the end of the mth stress increment in the $(N+1)$th cycle is,

$$\varepsilon_m^{N+1}=\varepsilon_{res}^{N}+\sum_{i=1}^{m}\frac{d\sigma/E_0}{f_1(\varepsilon_{i-1}^{N+1})} \tag{12}$$

where ε_{i-1}^{N+1} is the strain at the end of the $(i-1)$th stress increment in the $(N+1)$th cycle, and ε_{res}^{N} is the residual strain accumulated at the end of the Nth cycle. In the primary residual strain regime, ε_{res}^{N} was the primary residual strain accumulated at the end of the Nth cycle. In the secondary residual strain regime,

[5]The secondary residual strain accumulation rate has been defined by $d\varepsilon_{res}^{\sec}/dN$ instead of $d\varepsilon_{res}^{\sec}/dN^{\sec}$, since the rates were estimated from ε_{res} vs N plots (see Figure 5), and $d\varepsilon_{res}^{\sec}/dN$ simply reflects the slope of the ε_{res} vs N in the secondary phase. Moreover in the secondary residual strain accumulation phase $dN=dN^{\sec}$ and the two expressions are equivalent.

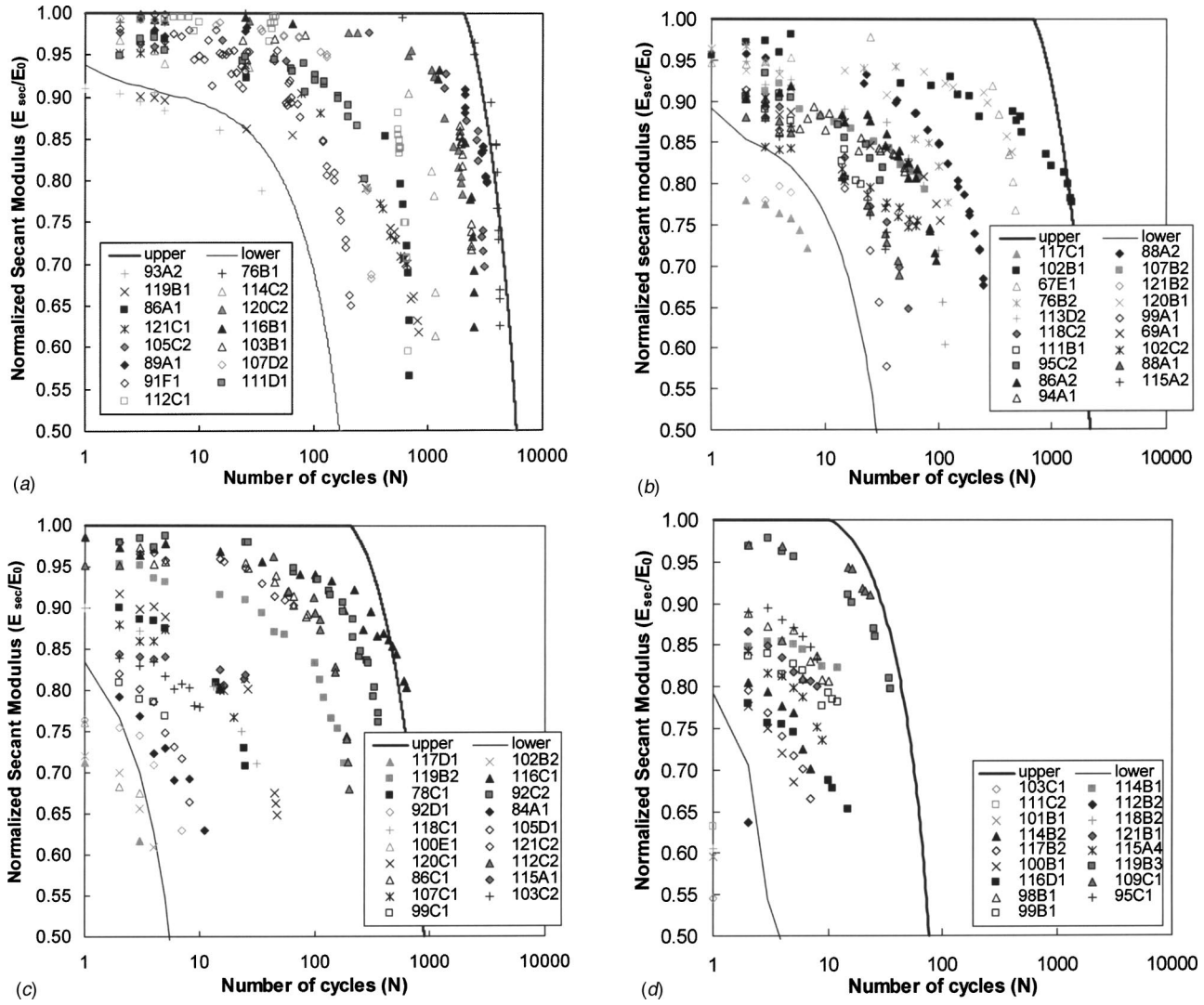

Fig. 7 Upper and lower bounds of the decrease of the normalized secant modulus predicted by the numerical model, for normalized stress ranges (*a*) (0.005, 0.006], (*b*) (0.006, 0.007], (*c*) (0.007, 0.008] and (*d*) (0.008, 0.009]. Note that upper and lower bound responses for both f_1 and f_2 have been considered in determining the model responses. The experimental points, identified by their sample numbers, have been included for comparison.

$$\varepsilon_{res}^{N} = \varepsilon_{res}^{pr} + (N - N^{pr}) \frac{d\varepsilon_{res}^{\sec}}{dN} \tag{13}$$

An objective of the model was to predict the bounds for the experimentally observed variation in the trabecular bone normalized secant modulus ($E_{\sec}/E_0$) as a function of the number of cycles (N). As explained above, the experimental data were divided into four normalized stress ranges: (0.005, 0.006], (0.006, 0.007], (0.007, 0.008], (0.008, 0.009]. The actual maximum and minimum normalized stresses observed in each of these ranges are shown in Table 1. For an upper bound model of $E_{\sec}/E_0$ vs. N, the minimum normalized stress at each range (i.e., 0.0053, 0.0061, 0.0072 and 0.0083, respectively) was defined as the characteristic normalized stress for the numerical model. Similarly, the maximum normalized stress (0.0059, 0.0069, 0.008 and 0.0087, respectively) was assumed to be the characteristic normalized stress for the lower bound model. In addition, the upper bound model used the upper and lower bounds of f_1 and f_2 (for the given stress range, see Table 1) respectively, while the lower bound model used the lower and upper bounds of f_1 and f_2, respectively. The primary residual strain accumulation characteristic (ε_{res}^{pr}) was defined based on the median value for the given normalized stress range, and is shown in Table 1. For all the generated curves, the unloading from the maximum stress (and maximum strain) level to zero-stress (and predetermined residual strain, from Eq. (8)) level was assumed to be linear.

4.3 Model Results. Figure 7 shows the numerical model predicted upper and lower bound $E_{\sec}/E_0$ vs. N curves for the four normalized stress ranges. The numerically predicted upper bound shows that at all stress levels, the specimens could exhibit linear behavior (with secant modulus equal to the undamaged modulus) for several cycles, till the upper bound damage initiation strain (0.0097) was achieved. On the other hand, the secant modulus for the lower bound response was less than the undamaged modulus, for all normalized stress ranges, the lower bound damage initiation strain (0.0038) being lower than the specimen strain in the first cycle. Figure 7 also shows the experimental observations of secant modulus variation for the different normalized stress ranges. The experimental points generally fell within the bounds defined by the numerical model.

5 Discussion: Applications of the Numerical Model

The present model was able to predict the bounds for the fatigue response of bovine trabecular bone. The initial modulus of the fatigue specimens used in the analysis ranged from ~0.9 −3.8 GPa. Thus, the present model is valid for a wide range of bovine trabecular bone moduli, and through elastic moduli-density correlations [29–31], may be applicable to a wide range of bone densities. Keaveny et al. [32] have shown that the characteristics of damage progression in human trabecular bone is similar to that of the bovine trabecular bone. Thus, the present model may potentially be applied to the analysis of fatigue trends in human trabecular bone. The model was able to combine complimentary information from the monotonic and the cyclic compression tests to predict the variation of normalized secant modulus with increasing cycles (at given normalized stress ranges). This is one of the strengths of the model, and as discussed below, may allow for the fatigue characteristic prediction from limited cyclic data. In addition, the model presents a convenient way for estimating the endurance limit of bovine trabecular bone, through suitable modification of Eq. (11).

5.1 Predictability of Fatigue Characteristics From Limited Cyclic Data. The inputs to the numerical model were (a) material response to increasing strain (f_1), estimated from the change in secant modulus, and (b) loading effect in terms of primary and secondary residual strain accumulation (f_2). The material response was determined from the monotonic stress-strain curves. The only input that was based on the cyclic compression experiments was related to the mechanism of residual strain accumulation. The success of the model in predicting the bounds of the experimentally observed E_{sec}/E_0 vs. N variation raises the possibility of trabecular bone fatigue characteristics determination based on relatively few cyclic tests. The reduction of E_{sec}/E_0 with increasing strain may be determined from comparatively economical monotonic compression experiments, while the cyclic compression tests will estimate the residual strain accumulation rates. In addition, the cyclic compression tests may be limited to low number of cycles ($N<500$), since the secondary residual strain accumulation rate ($d\varepsilon_{res}^{sec}/dN$) is relatively constant for a given specimen.

The predictability of trabecular bone fatigue characteristics from relatively few cyclic experiments is dependent on the accuracy of estimating the primary and secondary residual strain accumulation. As shown in Table 1 and Fig. 6, the residual strain accumulation for a given normalized stress range varies from specimen to specimen. Fewer cyclic tests may thus translate to inaccurate estimation of the bounds of residual strain variation, and its effect on the E_{sec}/E_0 vs. N prediction needs to be estimated. The effect of the error in primary residual strain estimation can be determined by calculating the change in predicted number of cycles when the primary residual strain at each stress range was estimated by the maximum or minimum value instead of the median value (see Table 1). For each of the four normalized stress ranges, the number of incremental cycles due to changes in primary residual strain was small compared to the upper estimates of the model. The effect of erroneous prediction of the primary residual strain accumulation (due to few cyclic experiments) on the model prediction may thus be limited.

The effect of the change in secondary residual strain accumulation rate estimates on the model predictions (N) may be estimated from Eq. (8). Assuming a given material model (f_1 constant), a normalized stress level ($\Delta\sigma/E_0$ constant), a constant ε_{res}^{pr}, and a relatively high N ($N \gg N^{pr}$), the number of cycles (N) corresponding to a given E_{sec}/E_0 is related to the secondary residual strain accumulation rate ($d\varepsilon_{res}^{sec}/dN$) by

$$N\frac{d\varepsilon_{res}^{sec}}{dN} = \text{constant} \tag{14}$$

$$\frac{N_2}{N_1} = \frac{\left(\frac{d\varepsilon_{res}^{sec}}{dN}\right)_1}{\left(\frac{d\varepsilon_{res}^{sec}}{dN}\right)_2} \tag{15}$$

where, secondary residual strain accumulation rates of $(d\varepsilon_{res}^{sec}/dN)_1$ and $(d\varepsilon_{res}^{sec}/dN)_2$ would reduce the normalized secant modulus to the given E_{sec}/E_0 at N_1 and N_2 cycles respectively. At all the stress levels, the maximum $d\varepsilon_{res}^{sec}/dN$ was approximately one to two orders of magnitude higher than the minimum $d\varepsilon_{res}^{sec}/dN$ (see Table 1), and N_{max} may be one to two orders of magnitude higher than N_{min} at a given stress level, if the same f_1 model is assumed in both cases. Thus, if the $d\varepsilon_{res}^{sec}/dN$ estimated from a single cyclic test is used to predict the E_{sec}/E_0 vs. N bounds, the predicted N may be as much as one to two orders of magnitude higher (or lower) than one of the previously defined bounds (i.e. the bounds shown in Fig. 7). However, a limited number of cyclic tests can be used to approximate the limits of E_{sec}/E_0 vs. N curves, even if a single characteristic $d\varepsilon_{res}^{sec}/dN$ value (rather than the bounds of the rates used in the present analysis) is used for the E_{sec}/E_0 vs. N estimates. This was evident in E_{sec}/E_0 vs. N estimates from the numerical model using a constant residual strain accumulation rate for a given normalized stress range. Figure 8 compares the numerical estimates (with $d\varepsilon_{res}^{sec}/dN$ defined by the median of the experimental data at each normalized stress range), with experimental E_{sec}/E_0 vs. N variation in the (0.005, 0.006] and (0.008, 0.009] normalized stress ranges. Although the calculated bounds defined a narrower range than those predicted using upper and lower bounds for $d\varepsilon_{res}^{sec}/dN$ (Fig. 7) and some of the experimental points fell outside the numerical bounds, the numerical predictions were relatively accurate in defining the experimental bounds at low damage levels (e.g. for $E_{sec}/E_0 = 0.9$). The difference between the numerically predicted bounds and the extrema of the experimental observations over the entire E_{sec}/E_0 range was less than an order of magnitude.

5.2 Estimation of the Endurance Limit. The change in the number of cycles (corresponding to a given loss of modulus) with change in the normalized stress level may be estimated from the present model. From Eq. (11),

$$N = \frac{f_1^{-1}(E_{sec}/E_0) - \varepsilon_{res}^{pr} - \left(\frac{\Delta\sigma/E_0}{E_{sec}/E_0}\right)}{f_2(\Delta\sigma/E_0)} + N^{pr} \tag{16}$$

An estimation of the bounds of the f_2 function is required in order to evaluate N at any given normalized stress. The bounds of the f_2 function over all normalized stress ranges, and the best-fit equations are shown in Fig. 6. The equations defining the best-fit lines were

$$\text{Upper bound:} \quad \frac{d\varepsilon_{res}^{sec}}{dN} = 3.0\times 10^{19}\left(\frac{\Delta\sigma}{E_0}\right)^{10.72} \tag{17}$$

$$\text{Lower bound:} \quad \frac{d\varepsilon_{res}^{sec}}{dN} = 3.0\times 10^{16}\left(\frac{\Delta\sigma}{E_0}\right)^{9.9} \tag{18}$$

In the normalized stress range (0.005–0.009], the upper and lower bounds of f_2 can be directly determined from Eqs. (17) and (18). Assuming that f_2 is continuous in the lower normalized stress levels, the bounds of the function at those stresses can be estimated by extrapolating the above equations. The upper and lower bound estimates at different normalized stresses ranging from 0.002 to 0.01 are shown in Table 2.

Figure 9 shows the predicted bounds of N (from Eq. (16)) corresponding to a 10% loss in secant modulus, for normalized stresses in the 0.002 to 0.01 range. The value of the primary residual strain, ε_{res}^{pr} was assumed to be 0.0007 for cyclic loadings

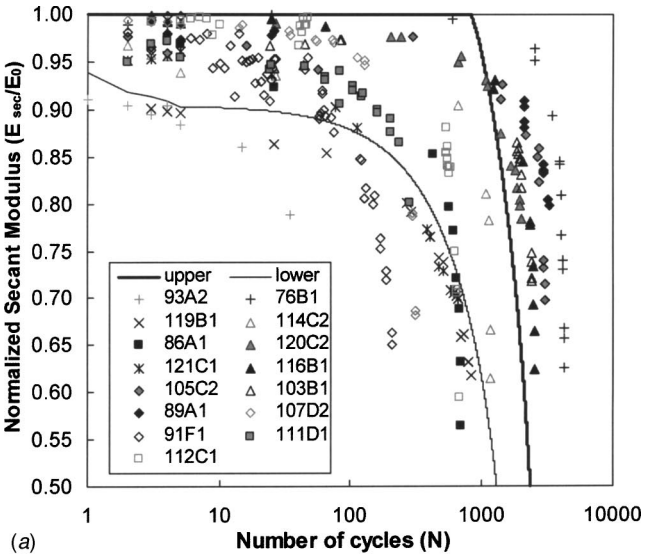

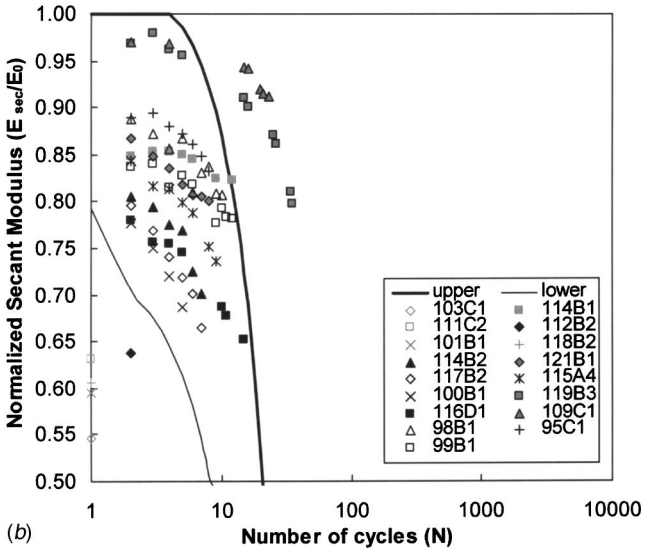

Fig. 8 Numerical model prediction of the upper and lower bounds of the normalized secant modulus reduction, at normalized stress ranges (*a*) (0.005, 0.006] and (*b*) (0.008, 0.009]. Note that for the model bound constructions, upper and lower bound responses for f_1 and a median response for f_2 (see Table 1) was assumed. The experimental points, identified by their sample numbers, have been included for comparison.

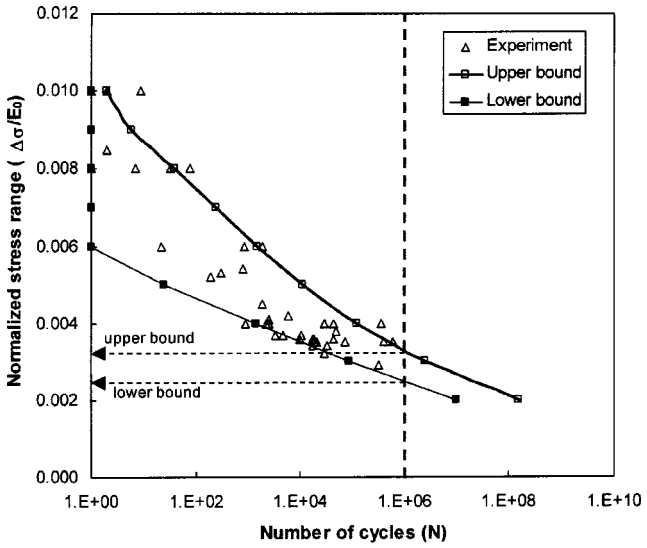

Fig. 9 The predicted *S-N* curve for bovine trabecular bone. The dotted line signifies the number of cycles corresponding to the endurance limit. The lower and upper bounds for the endurance limit are shown in the figure. The experimental data reflect cyclic compressive loadings of waisted samples of bovine trabecular bone [10].

at normalized stress equal to or less than 0.007 (this value was the median ε_{res}^{pr} value for the cyclic tests in the (0.005, 0.006] and (0.006, 0.007] normalized stress ranges, see Table 1). For cyclic loadings at normalized stress of 0.008, 0.009 and 0.01, ε_{res}^{pr} was assumed to be 0.0011, 0.0013 and 0.0013 respectively. N^{pr} was conveniently assumed to be 1 for all the normalized stresses. This is in agreement with the observed experimental range (1–2 cycles) for normalized stresses greater than 0.006. The experimentally observed N^{pr} in the (0.005, 0.006] normalized stress range was slightly higher (2–5 cycles). However, for the upper bound predictions in this stress range, the number of cycles (>1000, see Figs. 7, 8) was high enough such that this difference could be neglected. The model predictions have been compared with experimental data from Bowman et al. [10], who conducted cyclic compressions on waisted bovine trabecular bone specimens. Most of the experimental points from that study fell within the bounds predicted by the present model.

One of the important characteristics that may be estimated from Fig. 9 is the endurance limit. For metallic materials, the endurance limit has been defined as the stress level at which the fatigue specimen can withstand a large number of cycles (the estimate of 'large' is somewhat arbitrary, varying from 10^6 to 10^8 [33,34]). In the present case, the endurance limit has been assumed to be the

Table 2 Predictions of the upper and lower bounds of the secondary residual strain accumulation rate (based on Eqs. 17–18) at different normalized stress levels.

Maximum normalized stress	Upper bound of secondary residual strain accumulation rate	Lower bound of secondary residual strain accumulation rate
0.010	1×10^{-2}	5×10^{-4}
0.009	4×10^{-3}	2×10^{-4}
0.008	1×10^{-3}	5×10^{-5}
0.007	2×10^{-4}	1×10^{-5}
0.006	5×10^{-5}	3×10^{-6}
0.005	6×10^{-6}	5×10^{-7}
0.004	6×10^{-7}	6×10^{-8}
0.003	3×10^{-8}	3×10^{-9}
0.002	4×10^{-10}	6×10^{-11}

normalized stress level at which the bovine trabecular bone specimens may withstand 10^6 cycles with less than 10% loss in modulus (the dotted line in Fig. 9). Endurance limit predictions using the above model would vary from specimen to specimen. However, the upper bound of the fatigue limit as predicted by the current model is $\Delta\sigma/E_0 = 0.0032$, while the lower bound is at $\Delta\sigma/E_0 = 0.0024$. These bounds are based on extrapolations on the curves defining the variation of the secondary residual strain accumulation rate with normalized stress (Eqs. 17–18), and are thus approximate estimates of the endurance limit. Experimental observations at lower normalized stresses ($\Delta\sigma/E_0 < 0.005$) are required for more accurate predictions of the endurance limit.

6 Conclusion

The experimental stress-strain curves were analyzed for bovine trabecular bone specimens tested under monotonic compression, as well as cyclic compression at normalized stresses varying from 0.005 to 0.009. The reduction in the normalized material modulus (E_{sec}/E_0) with increasing strain was similar for the monotonic and cyclic loadings, and was governed by the maximum strain. On the other hand, the accumulation of residual strain under cyclic loadings was observed to depend on the normalized stress range. The rate of residual strain accumulation (per cycle) was constant beyond the first few cycles. A phenomenological model for predicting the change in the normalized secant modulus (E_{sec}/E_0) of trabecular bone specimens with increasing number of cycles (N) was developed, based on the above experimental observations. The model predicted the upper and lower bounds of the E_{sec}/E_0 vs. N variation, for cyclic tests in the normalized stress ranges of (0.005, 0.006], (0.006, 0.007], (0.007, 0.008] and (0.008, 0.009]. The model predictions at each stress level compared well with corresponding experimental observations. The model approximated the bounds in the secant modulus variation (with strain) in the cyclic compression experiments using those observed in monotonic experiments. Thus, the model shows the validity of predicting E_{sec}/E_0 vs. N curves from relatively few cyclic compression experiments, with the invariant material characteristics being determined from simpler monotonic compression experiments. In addition, the constant residual strain accumulation rate (beyond the first few cycles) allows the cyclic experiments to be limited to relatively small number of cycles. The model was used to predict the bounds for the change in number of cycles (for 10% secant modulus loss) with change in normalized stress for trabecular bone, and the endurance limit was determined. The model predictions for compressive endurance limit of bovine trabecular bone specimens fell between $\Delta\sigma/E_0 = 0.0032$ and $\Delta\sigma/E_0 = 0.0024$.

Acknowledgments

The authors wish to thank the Ford Foundation, the Alberta Heritage Scholarship Fund, the Cambridge-MIT Institute, the Matoula S. Salapatas Chair in Materials Science and Engineering at MIT and the Natural Sciences and Engineering Research Council (NSERC) of Canada for financial assistance. PG also wishes to thank Prof. F.-J. Ulm at MIT for helpful discussions.

References

[1] Freeman, M. A. R., Todd, R. C., and Pirie, C. J., 1974, "Role of Fatigue in Pathogenesis of Senile Femoral Neck Fractures," J. Bone Jt. Surg., **56B**, pp. 698–702.
[2] Riggs, B. L., and Melton, L. J., 1995, "The Worldwide Problem of Osteoporosis: Insights Offered by Epidemiology," Bone (N.Y.), **17**, pp. S505–S511.
[3] Daffner, R. H., and Pavlov, H., 1992, "Stress Fractures: Current Concepts," Am. J. Roentgenol., **159**, pp. 245–252.
[4] Burr, D. B., Forwood, M. R., Fyhrie, D. P., Martin, R. B., Schaffler, M. B., and Turner, C. H., 1997, "Bone Microdamage and Skeletal Fragility in Osteoporotic and Stress Fractures," J. Bone Miner. Res., **12**, pp. 6–15.
[5] Giladi, M., Milgrom, C., Kashtan, H., Stein, M., Chisin, R., and Dizian, R., 1986, "Recurrent Stress Fractures in Military Recruits. One Year Follow-up of 66 Recruits," J. Bone Jt. Surg., **68B**, pp. 439–441.
[6] Matheson, G. O., Clement, D. B., McKenzie, D. C., Taunton, J. E., Llyod-Smith, D. R., and MacIntyre, J. G., 1987, "Stress Fractures in Athletes: A Study of 320 Cases," Am. J. Sports Med., **15**, pp. 46–58.
[7] Lane, J. M., Russell, L., and Khan, S. N., 2000, "Osteoporosis," Clin. Orthop., **372**, pp. 139–150.
[8] Silva, M. J., Keaveny, T. M., and Hayes, W. C., 1997, "Load Sharing Between the Shell and Centrum in the Lumbar Vertebral Body," Spine, **22**, pp. 140–150.
[9] Michel, M. C., Guo, X.-D. E., Gibson, L. J., McMahon, T. A., and Hayes, W. C., 1993, "Compressive Fatigue Behavior of Bovine Trabecular Bone," J. Biomech., **26**, pp. 453–463.
[10] Bowman, S. M., Guo, X. E., Cheng, D. W., Keaveny, T. M., Gibson, L. J., Hayes, W. C., and McMahon, T. A., 1998, "Creep Contributes to the Fatigue Behavior of Bovine Trabecular Bone," J. Biomech. Eng., **120**, pp. 647–654.
[11] Moore, T. L. A., and Gibson, L. J., 2003, "Fatigue of Bovine Trabecular Bone," J. Biomech. Eng. **125**, pp. 761–768.
[12] Haddock, S. M., Yeh, O. C., Mummaneni, P. V., Rosenberg, W. S., and Keaveny, T. M., 2000, "Fatigue Behavior of Human Vertebral Trabecular Bone," 46th Annual Meeting, Orthopaedic Research Society, pg. 733.
[13] Moore, T. L. A., and Gibson, L. J., 2003, "Fatigue Microdamage in Bovine Trabecular Bone," ASME J. Biomech. Eng., **125**, pp. 769–776.
[14] Moore, T. L. A., and Gibson, L. J., 2002, "Microdamage Accumulation in Bovine Trabecular Bone in Uniaxial Compression," ASME J. Biomech. Eng., **124**, pp. 63–71.
[15] Schaffler, M. B., Radin, E. L., and Burr, D. B., 1989, "Mechanical and Morphological Effects of Strain Rate on Fatigue of Compact Bone," Bone (N.Y.), **10**, 207–214.
[16] Burr, D. B., Turner, C. H., Naick, P., Forwood, M. R., Ambrosius, W., Hasan, M. S., and Pidaprati, R., 1998, "Does Microdamage Accumulation Affect the Mechanical Properties of Bone?," J. Biomech., **31**, pp. 337–345.
[17] Taylor, D., O'Brien, F., and Lee, T. C., 2002, "A Theoretical Model for the Simulation of Microdamage Accumulation and Repair in Compact Bone," Meccanica, **37**, pp. 397–406.
[18] Moore, T. L. A., O'Brien, F. J., and Gibson, L. J., 2004, "Creep Does Not Contribute to Fatigue in Bovine Trabecular Bone," ASME J. Biomech. Eng., **126**, pp. 321–329.
[19] Guo, X.-D. E., McMahon, T. A., Keaveny, T. M., Hayes, W. C., and Gibson, L. J., 1994, "Finite Element Modeling of Damage Accumulation in Trabecular Bone under Cyclic Loading," J. Biomech., **27**, pp. 145–155.
[20] Schaffner, G., Guo, X. E., Silva, M. J., and Gibson, L. J., 2000, "Modelling Fatigue Damage Accumulation in Two-dimensional Voronoi Honeycombs," Int. J. Mech. Sci., **42**, pp. 645–656.
[21] Makiyama, A. M., Vajjhala, S., and Gibson, L. J., 2002, "Analysis of Crack Growth in a 3D Voronoi Structure: A Model for Fatigue in Low Density Trabecular Bone," J. Biomech. Eng., **124**, pp. 512–520.
[22] Paris, P. C., and Erdogan, F., 1963, "A Critical Analysis of Crack Propagation Laws," ASME J. Basic Eng., **85**, pp. 528–534.
[23] Carter, D. R., and Caler, W. E., 1983, "Cycle-dependent and Time-dependent Bone Fracture With Repeated Loading," J. Biomech. Eng., **105**, pp. 166–170.
[24] Carter, D. R., and Caler, W. E., 1985, "A Cumulative Damage Model for Bone Fracture," J. Orthop. Res., **3**, pp. 84–90.
[25] Taylor, D., 2002, "Modelling of Fatigue Crack Growth at the Microstructural Level," Comput. Mater. Sci., **25**, pp. 228–236.
[26] Keaveny, T. M., Guo, X.-D. E., Wachtel, E. F., McMahon, T. A., and Hayes, W. C., 1994, "Trabecular Bone Exhibits Fully Linear Elastic Behavior and Yields at Low Strains," J. Biomech., **27**, pp. 1127–1136.
[27] Keaveny, T. M., Wachtel, E. F., Guo, X.-D. E., and Hayes, W. C., 1994, "Mechanical Behavior of Damaged Trabecular Bone," J. Biomech., **27**, pp. 1309–1318.
[28] Keaveny, T. M., Pinilla, T. P., Crawford, R. P., Kopperdahl, D. L., and Lou, A., 1997, "Systematic and Random Errors in Compression Testing of Trabecular Bone," J. Orthop. Res., **15**, pp. 101–110.
[29] Gibson, L. J., 1985, "The Mechanical Behavior of Cancellous Bone," J. Biomech., **18**, pp. 317–328.
[30] Keaveny, T. M., Morgan, E. F., Niebur, G. L., and Yeh, O. C., 2001, "Biomechanics of Trabecular Bone," Annu. Rev. Biomed. Eng., **3**, pp. 307–333.
[31] Morgan, E. F., Bayraktar, H. H., and Keaveny, T. M., 2003, "Trabecular Bone Modulus-Density Relationships Depend on Anatomic Site," J. Biomech., **36**, pp. 897–904.
[32] Keaveny, T. M., Wachtel, E. F., and Kopperdahl, D. L., 1999, "Mechanical Behavior of Human Trabecular Bone after Overloading," J. Orthop. Res., **17**, pp. 346–353.
[33] Suresh, S., 1991, Fatigue of materials, Cambridge University Press, Cambridge, U.K., p. 127.
[34] Lemaitre, J., 1992, A Course on Damage Mechanics, Springer-Verlag, p. 110.